Article

Developmental Cell

Mechanistic Basis of Organization of the Harmonin/USH1C-Mediated Brush Border Microvilli Tip-Link Complex

Graphical Abstract

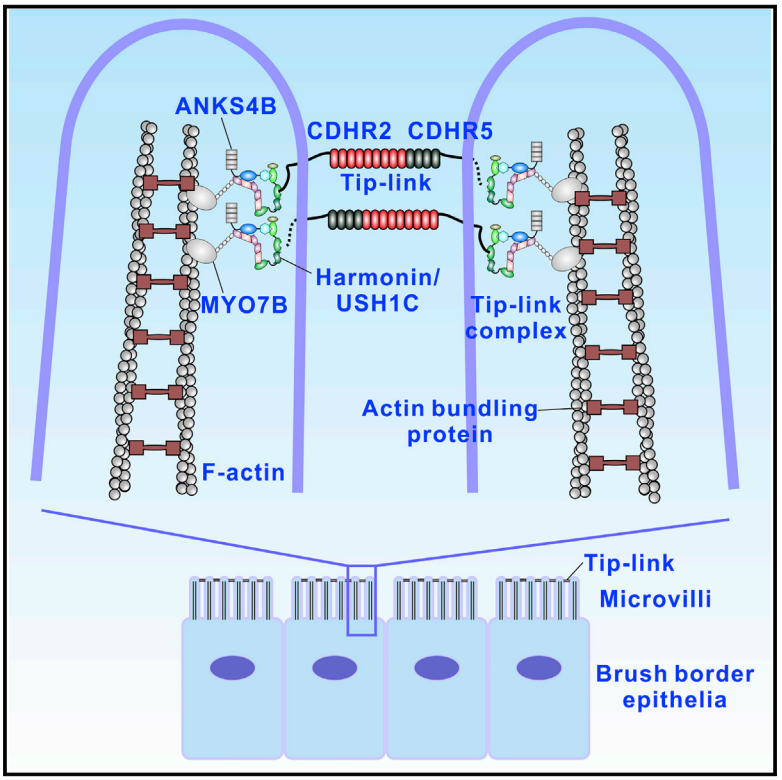

Authors

Jianchao Li, Yunyun He, Qing Lu, Mingjie Zhang

Correspondence

luqingtc@connect.ust.hk (Q.L.), mzhang@ust.hk (M.Z.)

In Brief

Li et al. present a systematic biochemical and structural characterization of the brush border inter-microvillar tip-link complex assembly, revealing its striking similarity with the inner ear hair cell inter-stereocilia complex organizations, despite their minimal overlap in proteins. The results provide mechanistic insight into the function of brush border microvilli under both normal physiological and disease conditions.

Highlights

- The brush border inter-microvilli link complex assembly is characterized
- The Harmonin/ANKS4B/Myo7B complex links cadherins with actin bundles
- Harmonin acts as the key scaffold of the inter-microvilli tip-link complex
- Despite minimal overlap, microvilli and stereocilia tip-link complexes are similar

Accession Numbers

5F3X
5F3Y

Li et al., 2016, Developmental Cell *36*, 179–189
January 25, 2016 ©2016 Elsevier Inc.
http://dx.doi.org/10.1016/j.devcel.2015.12.020

Developmental Cell
Article

Mechanistic Basis of Organization of the Harmonin/USH1C-Mediated Brush Border Microvilli Tip-Link Complex

Jianchao Li,[1,3] Yunyun He,[1,3] Qing Lu,[1,2,*] and Mingjie Zhang[1,2,*]
[1]Division of Life Science, State Key Laboratory of Molecular Neuroscience, Hong Kong University of Science and Technology, Clear Water Bay, Kowloon, Hong Kong, China
[2]Center of Systems Biology and Human Health, School of Science and Institute for Advanced Study, Hong Kong University of Science and Technology, Clear Water Bay, Kowloon, Hong Kong, China
[3]Co-first author
*Correspondence: luqingtc@connect.ust.hk (Q.L.), mzhang@ust.hk (M.Z.)
http://dx.doi.org/10.1016/j.devcel.2015.12.020

SUMMARY

Brush border microvilli are actin-based protrusions lining the apical surface of epithelial cells in intestines and proximal tubules of kidneys. While brush border microvilli resemble the relatively well-characterized stereocilia of hair cells, the mechanistic basis of tip-link complex organization in microvilli is poorly understood. Here, we have biochemically and structurally characterized the following pairs of interactions: protocadherin 24 and Harmonin (also known as USH1C or AIE-75), Harmonin and myosin VIIb (MYO7B), Harmonin and ANKS4B, and ANKS4B and MYO7B. We show that Harmonin, ANKS4B, and MYO7B form a stable ternary complex for anchoring microvilli tip-link cadherins. Despite having only Harmonin in common, the microvilli and the stereocilia tip-link complexes are formed via strikingly similar interaction modes. These results not only provide insight into the mechanistic bases of brush border microvilli formation and maintenance but may also be valuable for understanding some gut and/or kidney diseases caused by perturbations of brush border microvilli structures.

INTRODUCTION

Cell surface protrusions are important to cells in many aspects such as harvesting nutrients, sensing and responding to environmental stimuli, and navigating movements (Nambiar et al., 2010; Ridley, 2011). Based on their supporting core cytoskeletal structures, cellular protrusions can be divided into two groups, microtubule-based protrusions known as cilia and actin filament-based protrusions such as microvilli, stereocilia, and filopodia. Morphologically, microvilli and stereocilia share some common features. They are both assembled into bundle-like structures (Barr-Gillespie, 2015). Stereocilia are organelles located at the apical side of hair cells in cochlea, and are important for hearing and balance (Tilney et al., 1992). Many molecules that play critical roles in governing the development and maintenance of stereocilia have been identified and extensively studied (El-Amraoui and Petit, 2005; Pan and Zhang, 2012; Schwander et al., 2010). Mutations of genes encoding many of these molecules result in syndromic or non-syndromic deafness (Richardson et al., 2011). Among syndromic deafness, Usher syndrome I is the most severe form of heritable hearing and visual impairment disorders caused by mutations of one of five *USH1* genes (Mathur and Yang, 2015; Richardson et al., 2011). Microvilli are found at the apical surface of epithelial cells such as small intestines and kidney, and form densely packed bundle-like structures called brush borders (Louvard et al., 1992; Mooseker, 1985). Recent studies have shown that many of the protein components that regulate stereocilia development and maintenance have their corresponding counterparts in microvilli (Crawley et al., 2014b; McConnell et al., 2011), suggesting that the underlying molecular mechanisms for the development of stereocilia and microvilli might be similar (Crawley et al., 2014a).

In stereocilia, two Usher syndrome gene encoded cell adhesion proteins, protocadherin 15 (PCDH15, encoded by *USH1F*/*PCDH15*) and cadherin 23 (CDH23, encoded by *USH1D*/*CDH23*), form an inter-stereocilia linker called tip-link (Kazmierczak et al., 2007; Sotomayor et al., 2012). Microvilli also contain inter-microvillar links located near the apex of each microvillus, which are formed by two cadherin family proteins known as cadherin-related family member 2 (CDHR2, also known as protocadherin-24, encoded by *CDHR2*) and cadherin-related family member 5 (CDHR5, also known as mucin-like protocadherin, encoded by *CDHR5*) (Crawley et al., 2014b). CDH23 interacts with a scaffold protein called Harmonin through its cytoplasmic tail (Pan et al., 2009; Siemens et al., 2002; Wu et al., 2012). Harmonin, encoded by *USH1C*, is a multi-PDZ domain-containing protein and expresses in three major spliced isoforms known as Harmonin a, b, and c (Verpy et al., 2000). They all contain an N-terminal helical domain (NTD), followed by two PDZ domains and a predicted coiled-coil (CC) domain. The isoforms a and b contain an additional PDZ domain in their C termini. Harmonin b contains another predicted CC domain (CC2) and an unstructured proline-, serine-, and threonine-rich sequence which was reported to bind to F-actin (Boeda et al., 2002). Harmonin is also known

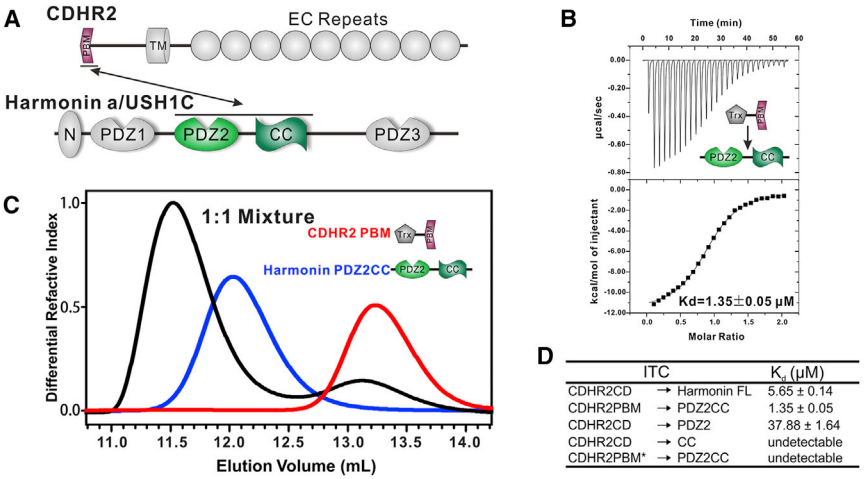

Figure 1. Biochemical Characterization of the CDHR2 and Harmonin Interaction

(A) Domain organizations of CDHR2 and Harmonin a.

(B) ITC result showing that CDHR2PBM binds to Harmonin PDZ2CC with K_d of ~1.35 μM.

(C) FPLC-based assay also showing that CDHR2PBM interacts with Harmonin PDZ2CC in solution.

(D) Summary of the binding affinities between different fragments of CDHR2 and Harmonin derived from ITC-based assays, showing that PBM and PDZ2CC were the minimal binding regions of the complex.

as autoimmune enteropathy-related 75-kDa antigen (AIE-75), and is highly expressed in the intestine and kidney (Kobayashi et al., 1998, 1999). Autoimmune enteropathy is a rare immune system disorder characterized by severe diarrhea and weight loss from malnutrition absorption (Kobayashi et al., 1999). Interestingly, it has been reported that the Usher syndrome patients with mutations in Harmonin also suffered from severe gastrointestinal symptoms and renal tubular dysfunction (Bitner-Glindzicz et al., 2000), indicating that Harmonin may also play important roles in formation and function of intestine and kidney brush border microvilli. Mirroring CDH23, CDHR2 has been reported to use its C-terminal PDZ binding motif (PBM) to interact with Harmonin PDZ in brush border microvilli (Crawley et al., 2014b), although the detailed interaction mode is not clear. In stereocilia, Harmonin forms a very stable tertiary complex with MYO7A (also known as unconventional myosin VIIa, encoded by *USH1B*) through the adaptor protein USH1G (also known as sans, encoded by *USH1G*) (Grati and Kachar, 2011; Pan and Zhang, 2012). MYO7A is scarce in microvilli. Instead its close homolog, MYO7B, is abundantly expressed in brush border microvilli (Chen et al., 2001; McConnell et al., 2011). Again, mirroring stereocilia, Harmonin has been found to associate with MYO7B (Crawley et al., 2014b). Curiously, microvilli are not known to express the adaptor protein USH1G, and thus how the membrane-anchored CDHR2/Harmonin complex is linked with the actin filament-attached MYO7B is not clear.

We have noted with interest that several epithelial tissues contain a protein highly similar to USH1G, called ankyrin repeat and SAM domain-containing protein 4B (ANKS4B, encoded by *ANKS4B*, also known as harmonin-interacting, ankyrin repeat-containing protein, harp). ANKS4B was originally identified in kidney (Johnston et al., 2004) and shares high similarity with USH1G, both in their sequences (40% sequence identity) and domain organizations. The Human Protein Atlas (http://www.proteinatlas.org/) showed that ANKS4B has the highest expression in intestine. The prominent expression of ANKS4B in intestine has also been confirmed by a recent proteomics study (Uhlen et al., 2015). Similar to USH1G, ANKS4B contains a type I PBM in its C terminus, and was reported to interact with Harmonin PDZ1 in a PBM-dependent manner (Johnston et al., 2004). Thus, it is possible that ANKS4B may act as an adaptor protein between Harmonin and MYO7B in brush border, similarly as USH1G does for linking Harmonin and MYO7A in stereocilia.

Here, using a combination of structural and biochemical approaches, we show that one of the components of the inter-microvillar link, CDHR2, uses its cytoplasmic tail PBM to bind to the PDZ2-CC region of Harmonin. We demonstrate that ANKS4B acts as an adaptor linking Harmonin and MYO7B. The C-terminal SAM domain and PBM of ANKS4B together interact with the Harmonin NTD-PDZ1 supramodule, and the structure of the complex solved here reveals the atomic details of the interaction. We further show biochemically and structurally that the central region of ANKS4B binds to the N-terminal MyTH4-FERM-SH3 supramodule of MYO7B with a mechanism highly analogous to the interaction between USH1G and MYO7A. Finally, we demonstrate that an extended PDZ3 of Harmonin binds to the C-terminal MyTH4-FERM tandem of MYO7B, revealing an unexpected binding mode both for PDZ domains and for MyTH4-FERM tandems. Our study represents a comprehensive mechanistic characterization of the inter-microvillar tip-link complex assembly in the cytoplasmic face. The results presented in this study will be valuable for understanding the development and maintenance of brush border microvilli and for understanding gastrointestinal and/or kidney diseases resulting from brush border microvilli defects due to malfunctioning of the proteins characterized herein.

RESULTS

CDHR2 Interacts with Harmonin through Its C-Terminal PBM

A recent breakthrough study has shown that CDHR2 and CDHR5 interact with each other to form the inter-microvillar link located at the apex of intestine brush border microvilli, and the cytoplasmic tails of these two cadherins associate with Harmonin (Crawley et al., 2014b). We first sought to characterize the detailed interactions governing the connection between Harmonin and the cadherins. The cytoplasmic tail of CDHR2 contains a conserved PBM (Figure 1A), and the cytoplasmic tail of CDHR5 is not conserved. Thus, we reasoned that the cytoplasmic domain (CD) of CDHR2 may directly bind to Harmonin, and CDHR5 may not interact with Harmonin. Indeed, we found, using purified

Table 1. Details of the Proteins and Their Boundaries Used in the Study

Protein Name	Amino Acid Residue Boundary
CDHR2 *Mus musculus* (Uniprot: E9Q7P9)	
CDHR2CD	1,176–1,308
CDHR2PBM	1,291–1,308
CDHR2PBM*	1,291–1,307
Harmonin a *Homo sapiens* (Uniprot: Q9Y6N9)	
NPDZ1	1–194
PDZ2	208–299
PDZ2CC	193–383
CC	300–383
NC-extended-PDZ3	428–552
PDZ3 N extension	428–449
PDZ3 C extension	537–552
N-extended PDZ3	428–542
ANKS4B *Mus musculus* (Uniprot: Q8K3X6)	
SAM-PBM	345–423
CEN	253–352
CEN1	253–330
CEN2	331–352
MYO7B	
NMFS *Mus musculus* (Uniprot: Q99MZ6)	962–1,578
CMF *Homo sapiens* (Uniprot: Q6PIF6)	1,582–2,116
MYO7A *Mus musculus* (Uniprot: P97479-2)	
NMFS	965–1,649
CMF	1,650–2,215
USH1G *Homo sapiens* (Uniprot: Q495M9)	
CEN	295–390
CDHR5 *Mus musculus* (Uniprot: Q8VHF2)	
CD	663–831

*indicates mutation of PBM by deleting the last residue.

recombinant proteins, that the entire CDHR2CD binds to the full-length Harmonin with a dissociation constant (K_d) of ~5.7 μM (Figures 1D and S1A; the construct details of all recombinant proteins used in this study are summarized in Table 1 for both clarity and easy comparison), a value typical for a canonical PDZ/PBM interaction (Ye and Zhang, 2013). In contrast, no interaction could be detected between CDHR5 CD and Harmonin (Figure S1B). Further detailed mapping experiments revealed that CDHR2 PBM binds to the PDZ2 and CC regions (PDZ2CC) of Harmonin (Figures 1B–1D). Analytical gel filtration chromatography (fast protein liquid chromatography [FPLC]) assay also showed that CDHR2 PBM and Harmonin PDZ2CC can interact with each other (Figure 1B). The isothermal titration calorimetry (ITC)-based assay showed that CDHR2 PBM binds to Harmonin PDZ2CC with a K_d of ~1.4 μM (Figure 1C). Removal of CC from PDZ2CC weakens the binding to a K_d of ~38 μM, and the CC domain alone has no detectable binding to CDHR2CD (Figure 1D). The weak interaction between Harmonin PDZ2 and CDHR2CD is consistent with the result in the previous study by Crawley et al. (2014b) showing that PDZ2 alone could not be pulled down by CDHR2CD. Finally, a 17-residue synthetic peptide corresponding to the CDHR2PBM but missing the last residue (i.e. residues 1,291–1,307 of CDHR2, referred to as CDHR2PBM*) had no detectable binding to Harmonin PDZ2CC (Figure 1D), indicating that CDHR2PBM is indispensable for the CDHR2/Harmonin interaction. In conclusion, similar to the interaction between CDH23 PBM and Harmonin PDZ2 in stereocilia, CDHR2 PBM also binds to Harmonin PDZ2, albeit that the interaction between CDHR2 and Harmonin also requires the CC region following Harmonin PDZ2. At this stage, we do not understand how the CC region enhances Harmonin PDZ2's binding to CDHR2CD as we have not been able to obtain diffracting-quality crystals of the Harmonin PDZ2CC/CDHR2PBM complex. The CC region may directly participate in the PDZ2CC/CDHR2PBM interaction. Alternatively, the CC region may simply facilitate folding and stability of Harmonin PDZ2, forming an extended PDZ domain (Wang et al., 2010; Ye and Zhang, 2013).

ANKS4B Binds to Harmonin in a Mode Highly Similar to that of USH1G

ANKS4B, similar to USH1G, consists of four N-terminal ANK repeats, a central region, and a sterile α motif (SAM) followed by a C-terminal type I PBM (Figure 2A). In a previous study, the crystal structure of Harmonin NPDZ1/USH1G SAM-PBM complex showed that Harmonin NTD, PDZ1, and a short C-terminal extension form a supramodule to interact with USH1G SAM-PBM with very high affinity (Yan et al., 2010). Taking into account the high similarity between ANKS4B and USH1G (Figure 2D), we wondered whether ANKS4B SAM-PBM might also interact with Harmonin NPDZ1 using the same binding mode. Since NPDZ1 tends to form aggregate in low-salt concentration buffer (e.g. 100 mM NaCl) and the protein adopts as a stable monomer in high-salt concentration buffers (Yan et al., 2010), all the experiments involving NPDZ1 described in this work were performed in buffer containing 500 mM NaCl. As such, the corresponding bindings are likely to be even stronger if measured under physiological salt concentrations. ITC-based assay indeed detected a very strong interaction between Harmonin NPDZ1 and ANKS4B SAM-PBM with K_d of ~3 nM (Figure 2B), which is comparable with the interaction between Harmonin NPDZ1 and USH1G SAM-PBM (K_d ~1.3 nM) (Yan et al., 2010). FPLC coupled with static light scattering (FPLC-SLS) assay demonstrated that Harmonin NPDZ1 and USH1G SAM-PBM form a stable complex with a 1:1 stoichiometry (Figure 2C).

To elucidate the atomic basis of the Harmonin/ANKS4B interaction, we solved the crystal structure of the Harmonin NPDZ1/ANKS4B SAM-PBM complex at 2.65 Å resolution (Table S1). The PBM of ANKS4B inserts into the groove formed by αB and βB of Harmonin PDZ1, and the ANKS4B SAM domain packs with the exposed side of αB of Harmonin PDZ1 (Figure 2E). In addition to the expected interactions between the "0" and "−2" positions of ANKS4B PBM and Harmonin PDZ1, the invariable $Asp420_{PBM}$ at the "−3" position forms a salt bridge with $Arg103_{NPDZ1}$ (Figure 2F). The interaction between ANKS4B SAM domain and Harmonin PDZ1 is mediated via two pairs of salt bridges ($Lys407_{SAM}$-$Glu148_{PDZ1}$, $Arg408_{SAM}$-$Glu149_{PDZ1}$), several

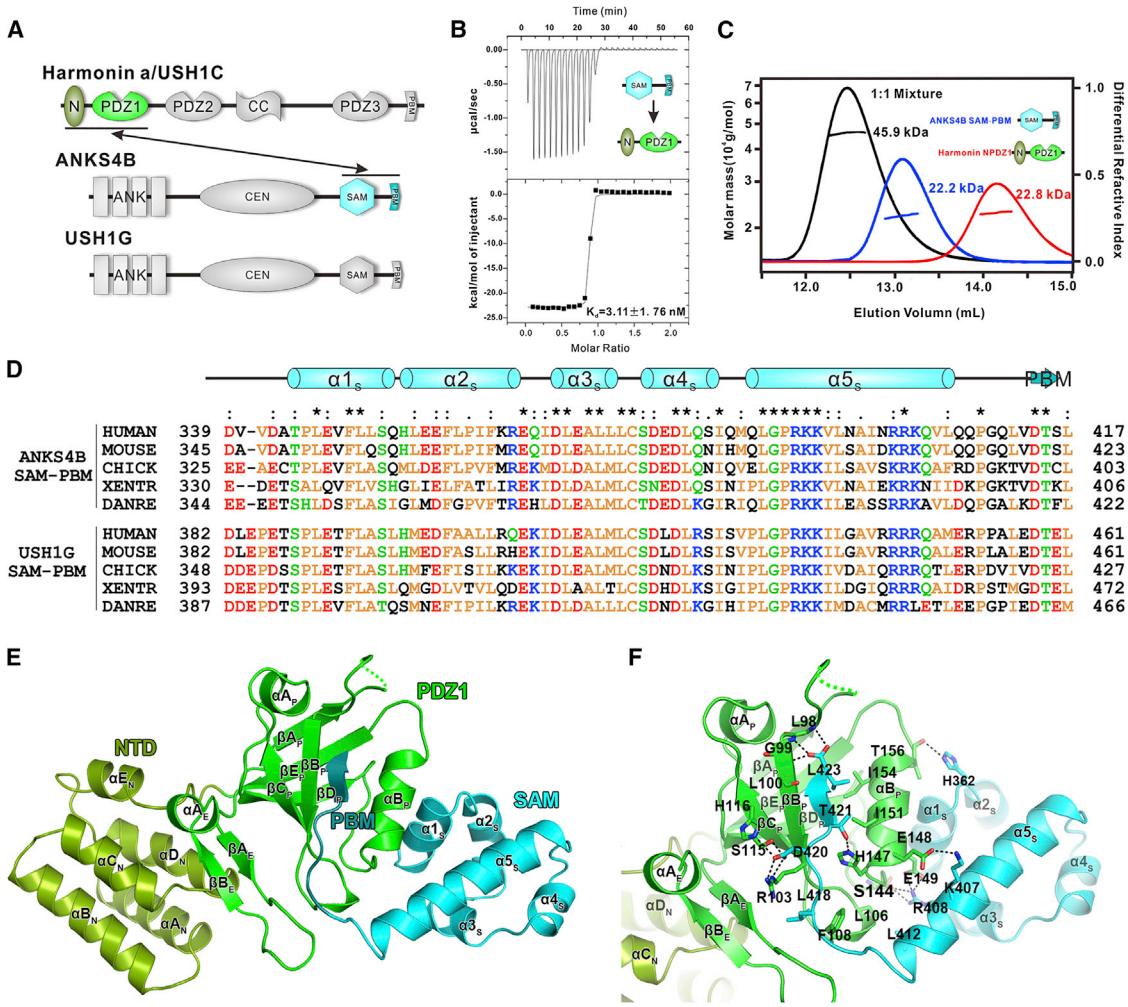

Figure 2. Biochemical and Structural Characterization of the ANKS4B and Harmonin Interaction

(A) Domain organizations of Harmonin, ANKS4B, and USH1G.

(B) ITC result showing that ANKS4B SAM-PBM binds to Harmonin NPDZ1 with a very strong affinity (K_d ~3 nM).

(C) FPLC-SLS analysis showing that ANKS4B SAM-PBM and Harmonin NPDZ1 formed a stable, 1:1 stoichiometric complex in solution.

(D) Sequence alignment of ANKS4B SAM-PBM and USH1G SAM-PBM from different vertebrate species. The symbols above the sequences are defined as follows: an asterisk (*) indicates positions with a fully conserved residue; a colon (:) indicates conservation between groups of strongly similar properties; a period (.) indicates conservation between groups of weakly similar properties.

(E) Overall structure of the ANKS4B SAM-PBM/Harmonin NPDZ1 complex.

(F) Combined stick and ribbon models showing the interaction details between ANKS4B SAM-PBM and Harmonin NPDZ1.

hydrogen bonds (side chain of $Gln361_{SAM}$ and side chain of $Asn152_{PDZ1}$, side chain of $His362_{SAM}$ and backbone carbonyl of $Thr156_{PDZ1}$, side chain of $Arg408_{SAM}$ and backbone carbonyl of $Ser144_{PDZ1}$), and hydrophobic interactions ($Leu412_{SAM}$-$Leu106_{PDZ1}$, $Leu418_{SAM}$-$Phe108_{PDZ1}$) (Figure 2F). The combined PDZ/PBM and PDZ/SAM interactions presumably lead to the formation of the highly stable Harmonin/ANKS4B complex. The residues from ANKS4B SAM-PBM that are involved in the interaction with Harmonin NPDZ1 can also be found in the corresponding positions in USH1G SAM-PBM (Yan et al., 2010) (Figure 2D). Not surprisingly, the overall structure of the Harmonin NPDZ1/ANKS4B SAM-PBM complex is essentially the same as that of the Harmonin NPDZ1/USH1G SAM-PBM complex (root-mean-square deviation of 0.71 Å, Figure S2).

An earlier study reported that Harmonin NPDZ1 (denoted "PDZ1" by the authors), but not PDZ2 and PDZ3, can bind to CDHR2CD (Crawley et al., 2014b). We tried to verify these results using purified proteins. ITC-based assay of the interaction between CDHR2CD and Harmonin NPDZ1 in the high-salt buffer detected a K_d of ~22 µM (Figure S3A), suggesting NPDZ1 can indeed bind, albeit weakly, to CDHR2CD (about 20 times weaker than the CDHR2CD/PDZ2CC interaction assayed in buffer containing 100 mM NaCl, Figure 1B). However, it is possible that the high concentration of salt in the assay buffer might have weakened the binding. To verify this possibility, we quantified the binding affinities of CDHR2CD to PDZ2CC in the assay buffer containing 500 mM NaCl, and the resulting K_d was ~20 µM (Figures S3B and S3C). Thus, NPDZ1 and PDZCC of Harmonin can

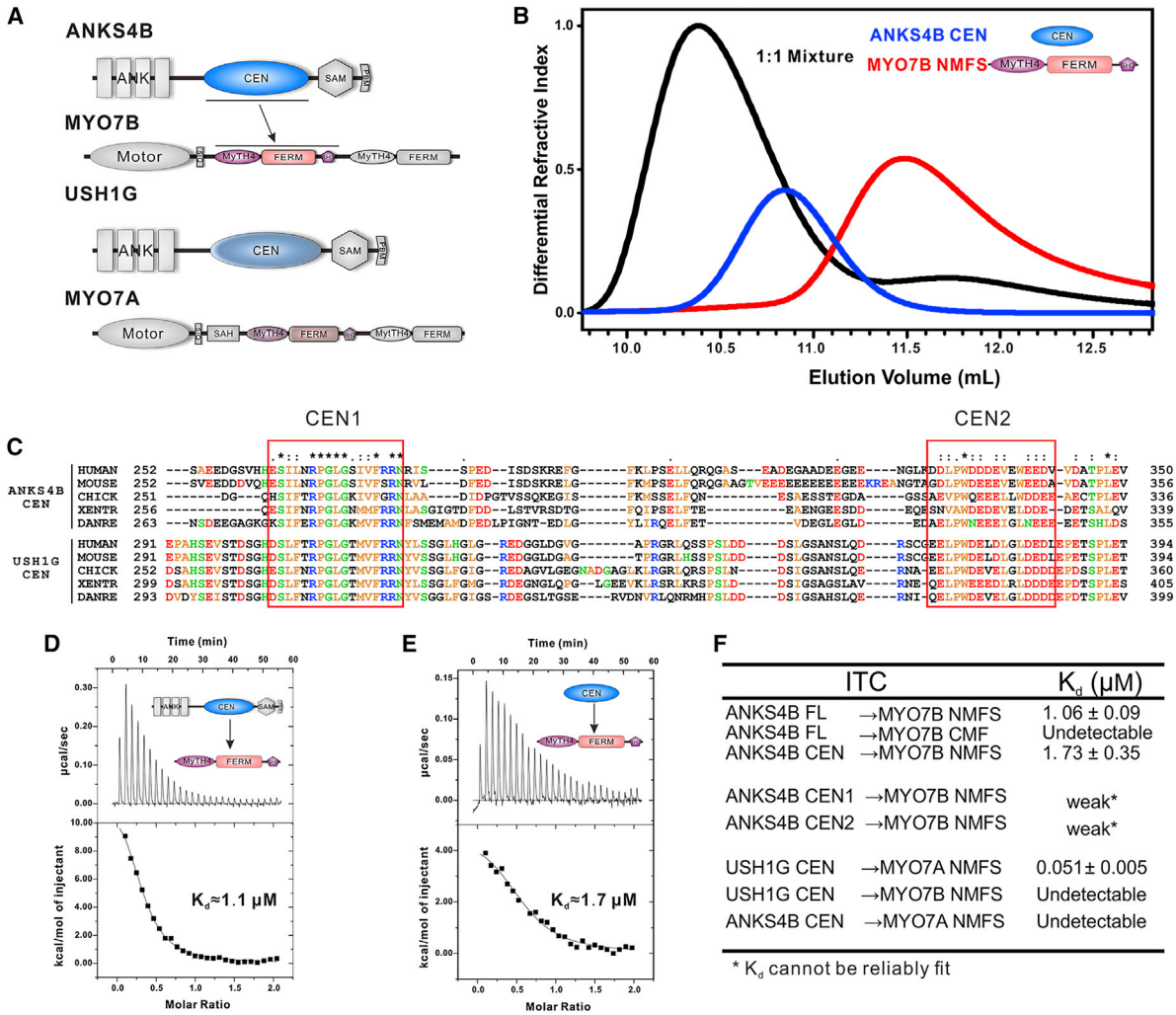

Figure 3. The Central Region of ANKS4B Binds to the N-Terminal MyTH4-FERM Tandem of MYO7B

(A) Domain organizations of ANKS4B, MYO7B, and their respective stereocilia counterparts USH1G and MYO7A.

(B) FPLC-based assay showing that ANKS4B CEN and MYO7B NMFS can interact with each other in vitro.

(C) Sequence alignment of the CEN regions of ANKS4B and USH1G from different species, showing that the boxed CEN1 and CEN2 regions are both highly conserved, whereas their flanking sequences are variable. The symbols above the sequences are the same as those defined in Figure 2D.

(D) ITC-based assay reveals that the full-length ANKS4B and MYO7B NMFS interact with each other with moderate affinity.

(E) ITC result shows that ANKS4B CEN had a similar binding affinity toward MYO7B NMFS compared with the full-length ANKS4B.

(F) Summary of ITC-derived binding affinities of different fragments of ANKS4B, MYO7B, USH1G, and MYO7A, showing that the ANKS4B/MYO7B and the USH1G/MYO7A interactions are each very specific.

bind to CDHR2CD with comparable affinities. However, the NPDZ1/SAM-PBM structure shows that the PBM-binding groove of Harmonin NPDZ1 is occupied by ANKS4B SAM-PBM, and the interaction between Harmonin NPDZ1/ANKS4B SAM-PBM is nearly 10^4-fold stronger than the Harmonin NPDZ1/CDHR2CD interaction. Therefore, it is predicted that CDHR2 will not bind to Harmonin NPDZ1 in the presence of ANKS4B. Indeed, no binding could be detected when CDHR2PBM was used to titrate the NPDZ1/SAM-PBM complex (Figure S3D). In contrast, the binding of CDHR2CD to the full-length Harmonin complex is not affected by the presence of ANKS4B SAM-PBM (Figure S3E). Therefore, we believe that PDZ2CC of Harmonin is the bona fide binding site for CDHR2CD in brush border microvilli.

MYO7B N-Terminal MyTH4-FERM-SH3 Specifically Interacts with the ANKS4B CEN Region

In stereocilia, the USH1G CEN region interacts with the MYO7A N-terminal MyTH4-FERM domain (Wu et al., 2011), and the interaction serves to link the CDH23/Harmonin/USH1G complex with the actin filament bundles via MYO7A's motor head. We first compared the amino acid sequences of the central region of ANKS4B with those of USH1G (Figures 3A and 3C). Strikingly, the previously identified CEN1 and CEN2 regions of USH1G, which are directly responsible for binding to the MYO7A MyTH4-FERM tandem (Wu et al., 2011), are both highly conserved in ANKS4B (Figure 3C). MYO7B is the paralog of MYO7A (54% sequence identity), and is expressed primarily in kidney and intestine (Chen et al., 2001). Similar to MYO7A,

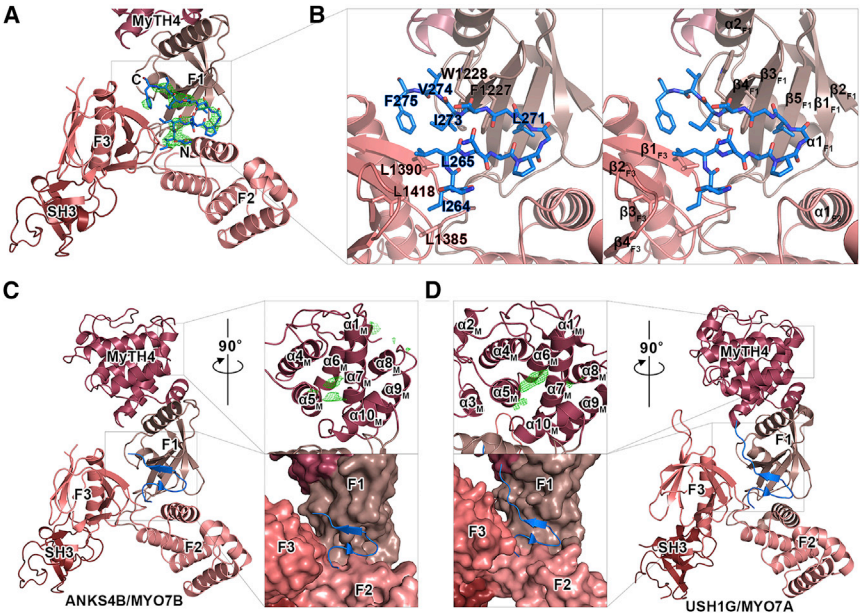

Figure 4. Structure of the ANKS4B CEN/MYO7B NMFS Complex

(A) Electron density of ANKS4B CEN1 in the ANKS4B CEN/MYO7B NMFS complex. The F_o-F_c map was calculated by omitting CEN1 from the final model and contoured at 3σ.

(B) Detailed interactions between ANKS4B CEN1 (with the stick model in blue) and MYO7B NMFS.

(C and D) Comparison of the ANKS4B CEN/MYO7B NMFS and the USH1G CEN/MYO7A NMFS structures, showing that ANKS4B and USH1G adopt similar binding modes toward the respective MYO7 NMFS.

MYO7B can be divided into three parts: the motor head, the neck region, and the tail cargo-binding domain. Curiously, MYO7B lacks the so-called single α helix that is found in MYO7A following its five IQ motifs. The tail region of MYO7B also consists of two MyTH4-FERM tandems separated by an SH3 domain (Figure 3A). Sequence alignment analysis showed that N-terminal MyTH4-FERM-SH3 (NMFS) of MYO7A and MYO7B are highly similar, and most of the residues that form the hydrophobic CEN1 binding groove in MYO7A NMFS can also be found in MYO7B NMFS (Figure S4). Therefore, we hypothesized that MYO7B NMFS might also be able to bind to the ANKS4B CEN region.

To test this hypothesis, we used ITC to measure the binding of the full-length ANKS4B to NMFS or C-terminal MyTH4-FERM (CMF) of MYO7B. We found that the NMFS binds to the full-length ANKS4B with a K_d of ~1.1 μM (Figure 3D), whereas no binding was detected between CMF and ANKS4B (Figure 3F). Next, we designed a fragment of ANKS4B CEN (amino acids 253–352, Figure 3C) with its boundary matching that of the USH1G CEN region (Wu et al., 2011). ITC assay showed that ANKS4B CEN binds to MYO7B NMFS with a K_d of ~1.7 μM (Figure 3E), indicating that the CEN region is sufficient for the ANKS4B/MYO7B interaction. In the FPLC study, the 1:1 mixture showed a significant peak shift, consistent with the binding showed by the ITC-based assays (Figure 3B). Moreover, the smaller than the predicted elution volume for ANKS4B CEN in the FPLC elution profile indicated that, similar to USH1G CEN (Wu et al., 2011), ANKS4B CEN also adopts an unfolded structure in solution (Figure 3B). We further separated CEN into two fragments, each containing the boxed CEN1 and CEN2 sequences shown in Figure 3C. ITC-based assay showed that both fragments can bind to MYO7B NMFS but with weaker affinity than the CEN region (Figure S5). Thus, both CEN1 and CEN2 directly interact with MYO7B NMFS, a mode similar to what was observed in the interaction between USH1G CEN and MYO7A NMFS (Wu et al., 2011) (Figure 3F).

To further understand the interaction between ANKS4B CEN and MYO7B NMFS, we determined the crystal structure of the MYO7B NMFS/ANKS4B CEN complex at 3.4 Å resolution (Table S1). The overall structure of MYO7B NMFS adopts a Y-shaped conformation, in which the MyTH4 domain physically interacts with FERM-F1 lobe, forming an intimately packed MyTH4-FERM tandem as observed in previously characterized myosin MyTH4-FERM tandems (Figure 4C) (Hirano et al., 2011; Wei et al., 2011; Wu et al., 2011). The SH3 domain also contacts the FERM-F3 lobe, although the relative position is different from that in MYO7A (the SH3 domain of MYO7B rotates by ~17° clockwise when the F3 lobes are superimposed, Figure 4C). Near the center of the "cloverleaf" of the FERM domain, the strong positive electron density allows us to build a β-hairpin structure corresponding to ANKS4B CEN1 (Figure 4A). The binding between ANKS4B CEN1 and MYO7B NMFS is dominated by hydrophobic interactions. Side chains of $Ile264_{ANKS4B}$ and $Phe275_{ANKS4B}$ from ANKS4B CEN1 make contacts with side chains of $Leu1385_{MYO7B}$, $Leu1390_{MYO7B}$, and $Leu1418_{MYO7B}$ from NMFS F3 lobe (Figure 4B). In addition, two bulky residues, $Phe1227_{MYO7B}$ and $Trp1228_{MYO7B}$ from NMFS F1 lobe, interact with $Leu270_{ANKS4B}$, $Ile273_{ANKS4B}$, and $Val274_{ANKS4B}$ (Figure 4B). The conformations and positions of ANKS4B CEN1 and USH1G CEN1 are very similar in their respective NMFS-bound state (Figures 4C and 4D). In the structure of MYO7A NMFS/USH1G CEN complex, the structure of CEN2 cannot be reliably determined by X-ray crystallography. However, sparse electron densities can be seen located near α5, α7, and α10 of the MyTH4 domain (Figure 4D), and these densities were shown to originate from USH1G CEN2 (Wu et al., 2011). Interestingly, discontinuous electron densities can also be seen at nearly the same positions of the MYO7B MyTH4 domain in the ANKS4B CEN/MYO7B NMFS complex (Figure 4C). Based on the high sequence similarities, we believe that these electron densities also originate from ANKS4B CEN2.

To determine whether the ANKS4B/MYO7B and USH1G/MYO7A interactions are specific, we tested the bindings between MYO7A NMFS and ANKS4B CEN and between MYO7B NMFS and USH1G CEN using ITC-based assays. No binding could be detected in either of these combinations (Figure 3F), indicating that the two highly homologous MYO7s can

specifically differentiate their respective targets USH1G and ANKS4B, which in their own rights are also highly similar to each other. Detailed analysis of the amino acid sequences and the two NMFS/CEN complex structures provides us with some hints regarding the binding specificity. Comparing the ANKS4B and USH1G CEN1 sequences, we find two differences: the corresponding residue of $Leu265_{ANKS4B}$ in ANKS4B is $Phe307_{USH1G}$ in USH1G (Figure 3C), which is conducive for making additional hydrophobic contacts to $Phe1473_{MYO7A}$ and $Ile1490_{MYO7A}$ in MYO7A; $Ser276_{ANKS4B}$ in ANKS4B is $Arg318_{USH1G}$ in USH1G (Figure 3C), which forms hydrogen bonding with $Ser1310_{MYO7A}$ and charge-charge interaction with $Asp1317_{MYO7A}$. These two substitutions may explain, at least in part, the significantly stronger binding between MYO7A and USH1G than between MYO7B and ANKS4B (50 nM versus 1 μM in their K_d values). Our current structure cannot provide details of the ANKS4B CEN2/MYO7B MyTH4 interaction, as we cannot define the structure of CEN2 based on the very scarce electron densities. Moreover, although the overall architectures of the FERM domains in the CEN-bound forms of the two MYO7 NMFS are quite similar (Figures 4C and 4D), the relative positions of the three lobes vary to some extent (the F2 and F3 lobes of MYO7B rotate ~7° anti-clockwise and ~10° clockwise, respectively, when their F1 lobes are superimposed). Such conformational difference of the FERM domain cloverleaf structures may also contribute to the target recognition specificity of the two motors' NMFS tandems. More broadly, the sensitivity of the target binding to the inter-lobe conformation of the three lobes of a FERM domain can have potential impact on FERM domain-mediated target binding diversity and specificity as well as possible allosteric regulations of FERM/target bindings.

Interaction between MYO7B C-Terminal MyTH4-FERM and Harmonin PDZ3

In stereocilia, MYO7A NMFS interacts with USH1G CEN with an affinity around 50 nM, 20 times stronger than that between MYO7B NMFS and ANKS4B CEN. We next asked whether there might be additional binding sites for the MYO7B tail to enhance the link between actin filament bound myosin and the highly stable ANKS4B/Harmonin complex. In an earlier study, it was reported that CDHR2CD directly interacts with the MYO7B tail (Crawley et al., 2014b). We used ITC to quantify the binding between CDHR2CD and the entire tail of MYO7B, and found the binding to be extremely weak (K_d ~140 μM). Such weak interaction between CDHR2CD and the MYO7B tail is not likely to be physiologically meaningful, as the affinity between CDHR2PBM and Harmonin PDZ2CC is about 100 times stronger (Figure 1B). It was reported that Harmonin can also directly bind to the MYO7B tail with an affinity stronger than the CDHR2/MYO7B interaction (Crawley et al., 2014b). Again, we used an ITC-based assay to verify this interaction, and found that the full-length Harmonin binds to the MYO7B C-terminal MyTH4-FERM tandem with a K_d of ~1.1 μM (Figure 5B). We further mapped the MYO7B CMF binding region of Harmonin to be an extended PDZ3 containing flanking sequences in both its termini (referred to as NCPDZ3, Figures 5A–5C). FPLC-based binding assay further confirmed the interaction between Harmonin NCPDZ3 and MYO7B CMF (Figure 5D).

Given the current knowledge about the canonical target binding modes of PDZ domains, the Harmonin NCPDZ3 and MYO7B-CMF interaction is highly unusual, as there is no PBM at the C terminus of MYO7B. The interaction is also unique for MyTH4-FERM tandems, as MyTH4-FERM tandems are not known to bind to a PDZ domain. We analyzed the atomic structure of Harmonin apo-PDZ3 deposited in the PDB (PDB: 1V6B), and found that the sequence we used contains an N-terminal extension forming a short α helix (N-extension) and a flexible C-terminal extension (C-extension, Figure S5). Both the N-extension and C-extension are conserved in Harmonins from fish to mammals (Figure S5). Deletion of the N-extension mildly decreased the binding affinity by ~4-fold, while deletion of the C-extension totally abolished the binding (Figure 5E). However, no bindings could be detected for either the N-extension or the C-extension alone (Figure 5E), indicating that the PDZ3 core provides the major binding energy for CMF while the two extensions (the C-terminal extension in particular) facilitate the binding. In an earlier glutathione S-transferase (GST) pull-down-based mapping study (Crawley et al., 2014b), PDZ3 was reported not to interact with the MYO7B tail. However, the sequence that the authors used (amino acids 360–534) lacked the entire C-terminal extension, which explains why no binding was detected. Thus, the PDZ3 together with its N-extension and C-extension form an integral extended PDZ domain to interact with MYO7B CMF. The detailed molecular basis governing this unexpected complex formation awaits the determination of the atomic structure of the complex.

To test whether the interaction between MYO7B CMF and Harmonin NCPDZ3 is specific for the brush border MYO7B, we used a GST pull-down assay to characterize the interaction between MYO7A and Harmonin. We used GST-tagged NCPDZ3 to pull down either the GFP-tagged MYO7A or GFP-tagged MYO7B expressed in heterologous cells. MYO7B CMF can be robustly pulled down by GST-NCPDZ3, whereas only a small amount of MYO7A CMF can be detected in the same assay (Figure 5F). Thus, despite the high similarity between MYO7A CMF and MYO7B CMF, the interaction between Harmonin NCPDZ3 and MYO7B is highly specific.

DISCUSSION

In this study, we performed systematic biochemical and structural characterizations of the protein interaction network residing at the cytoplasmic face of the brush border inter-microvilli tip-link. Our study includes detailed characterizations of previously reported protein-protein interactions between CDHR2 and Harmonin and between MYO7B and Harmonin (Crawley et al., 2014b). We have also discovered in this study that ANKS4B, a protein highly homologous to USH1G and abundantly expressed in brush border microvilli, functions as a key scaffold linking MYO7B with the Harmonin/CDHR2 complex. We have summarized the protein interaction network responsible for assembling the brush border inter-microvillar tip-link complex in Figure 6A. The brush border inter-microvillar tip-link complex assembly is strikingly similar to the inner ear stereocilia tip-link complex organizations (Figures 6A and 6B). They both utilize adhesive, heteromeric cadherin family proteins to build filamentous inter-microvillar/inter-stereocilia tip-links that can sustain mechanical

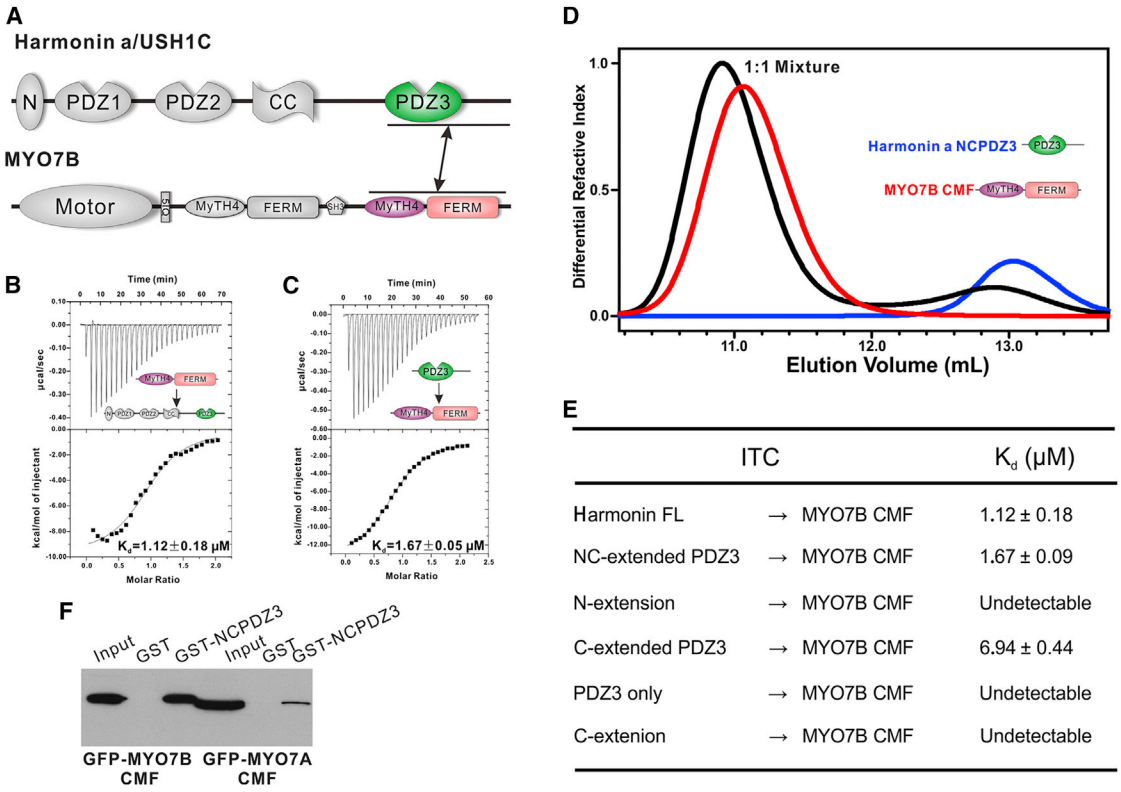

ITC		K_d (μM)
Harmonin FL	→ MYO7B CMF	1.12 ± 0.18
NC-extended PDZ3	→ MYO7B CMF	1.67 ± 0.09
N-extension	→ MYO7B CMF	Undetectable
C-extended PDZ3	→ MYO7B CMF	6.94 ± 0.44
PDZ3 only	→ MYO7B CMF	Undetectable
C-extenion	→ MYO7B CMF	Undetectable

Figure 5. The Extended PDZ3 Domain of Harmonin Binds to the MYO7B C-Terminal MyTH4-FERM Tandem

(A) Domain organizations of Harmonin and MYO7B.

(B) ITC-based assay shows that MYO7B CMF binds to the full-length Harmonin with moderate affinity.

(C) ITC result showing that Harmonin PDZ3 containing both N- and C-terminal extension sequences had affinity toward MYO7B CMF similar to that of the full-length Harmonin.

(D) FPLC-based assay showing that the extended PDZ3 of Harmonin and MYO7B CMF can form a complex in vitro.

(E) Summary of ITC-derived binding results of different fragments of Harmonin and MYO7B, showing that both N- and C-extensions of Harmonin PDZ3 are required for Harmonin to bind to MYO7B CMF.

(F) GST pull-down assay shows that Harmonin NCPDZ3 specifically binds to MYO7B CMF, but not to MYO7A CMF.

strains. Both systems use two scaffold proteins (Harmonin and ANKS4B in brush border, Harmonin and USH1G in inner ear) as the hub to organize the respective multi-protein complex within each microvilli/stereocilia. The multi-domain scaffold protein Harmonin appears to be particularly important. Via binding to the CD of cadherins, Harmonin provides an anchoring point for the inter-microvillar/inter-stereocilia cadherin complex. Through binding to MYO7, Harmonin serves as a bridge connecting the membrane-spanning cadherin complex with the microvilli/stereocilia actin bundles (Figures 6A and 6B, bottom panels).

Nonetheless, there are clear distinctions between these two systems. First, except for Harmonin, which is present in both complexes, the rest of the proteins forming the microvilli tip-link complex and those forming the stereocilia tip-link complex are different, although each protein in one system has a close homolog in the other. We have demonstrated in multiple cases that the interactions within each system are often very specific and not interchangeable. For example, the ANKS4B/MYO7B and USH1G/MYO7A interactions are specific within each pair, despite the overall structures of the two complexes and their interaction modes being highly similar. There also exists some unique interaction features within each of the two systems. In stereocilia, CDH23 interacts with Harmonin via multivalent interactions using its PBM and residues encoded by exon 68 (Pan et al., 2009; Wu et al., 2012). The cytoplasmic tail of CDHR2 uses its PBM to interact with an extended PDZ2 domain (PDZ2CC) of Harmonin. Interestingly, despite the above mechanistic differences, the overall binding affinities of the CDH23/Harmonin complex and the CDHR2/Harmonin complex are rather similar. It should also be noted that the binding pocket located in Harmonin NTD is unoccupied in the microvilli tip-link complex, suggesting that there might be additional Harmonin binding components remaining to be identified. In addition, the tripartite complex Harmonin/USH1G/MYO7A in stereocilia is formed by two pairs of very strong binary interactions between Harmonin and USH1G and between USH1G and MYO7A (Figure 6B). In microvilli, the binary interaction between ANKS4B and Harmonin is also very strong. However, the interaction between ANKS4B and MYO7B is much weaker than that between USH1G and MYO7A. Unique to the microvilli system, MYO7B forms another pair of interactions with the extended PDZ3 of Harmonin, also with moderate affinity. The simultaneous bindings of Harmonin and ANKS4B to MYO7B should ensure the formation of a highly

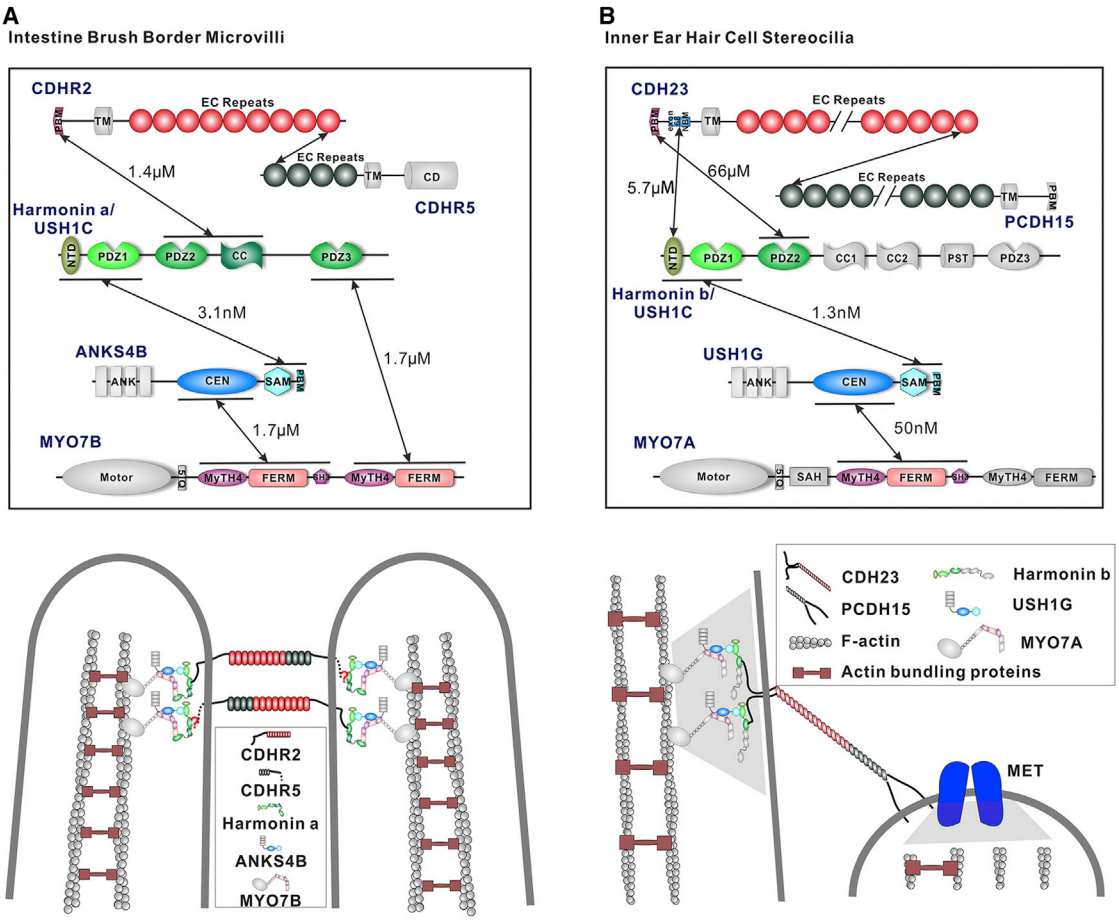

Figure 6. Summary and Comparison of the Tip-Link Protein-Protein Interaction Networks in Brush Border Microvilli and Inner Ear Stereocilia

(A) The top panel summarizes the detailed protein interaction network governing the assembly of the inter-microvillar tip-link. Except for the extracellular cadherin repeat-mediated hetero-dimerization interaction between CDHR2 and CDHR5 identified recently by Tyska's group (Crawley et al., 2014b), the rest of the interactions marked by two-way arrows have been characterized quantitatively in this study. The bottom panel is a cartoon summary of the protein interaction network in microvilli.

(B) The protein interaction network governing the inner ear stereocilia tip-link complex (also known as the USH1 complex) assembly. The figure is adapted from an earlier review by Pan and Zhang (2012). The bottom panel is a cartoon summary of the protein interaction network in stereocilia adapted from an earlier review by Lu et al. (2014).

stable Harmonin/ANKS4B/MYO7B complex in microvilli. Both the overall similarities and unique differences in organizing the microvilli and stereocilia tip-link complexes presumably are matched with the morphologically similar and functionally distinct properties of the two actin-based protrusions in animal kingdoms.

By comparing the proteomics studies between the brush border and inner ear hair bundles (McConnell et al., 2011; Shin et al., 2013), these two actin-based protrusion systems share many more common/homologous components in addition to the interaction networks discussed above. For example, several cytoskeleton-related proteins are present in both systems. Myosin 1c is known to be located in stereocilia and is important for adaptation of mechanical transductions (Gillespie and Cyr, 2004); myosin 1a (also known as brush border myosin I) has been reported to be important in brush border microvilli organization (Tyska et al., 2005). Espin, a well-known actin bundling protein, is important for the actin filament morphology in both systems (Sekerkova et al., 2006). Eps8, an actin capping protein known to play essential roles in stereocilia elongation (Manor et al., 2011), also is highly expressed in microvilli and is involved in the growth of microvilli. The striking similarities of the microvilli and stereocilia systems suggest that knowledge obtained from one system might be valuable for understanding the other. At present, our understanding of stereocilia tip-link complex is much more advanced than that of the brush border microvilli tip-link complex, at least partly due to clearly tractable clinical phenotypes and human genetics of the Ush1 syndromes, as well as powerful animal models that can model human diseases (Friedman et al., 2011; Gillespie and Muller, 2009; Richardson et al., 2011). We anticipate that the systematic mechanistic-based dissection of the brush border microvilli tip-link complex organization reported in this study can provide valuable insights for future functional studies of brush border microvilli in intestine and kidney. We hope that the protein interaction network characterized in our study may also be helpful in understanding

possible gut and/or kidney diseases caused by mutations of the genes encoding the proteins investigated in this work.

EXPERIMENTAL PROCEDURES

Constructs and Protein Expression

The Uniprot code of each protein and boundaries of recombinant proteins used in this study are summarized in Table 1. The genes encoding CDHR2CD, CDHR5CD, ANKS4B, and MYO7B NMFS were amplified by PCR from *Mus musculus* intestine cDNA and cloned into a pET vector. Fragments encoding Harmonin a and USH1G were amplified by PCR from *Homo sapiens USH1C* and *USH1G*, respectively, and cloned into a pET vector. Myosin VIIa fragments were PCR amplified from the mouse *USH1B* gene and cloned into a pET vector or pEGFP vector. The sequence encoding MYO7B CMF was amplified by PCR from the MYO7B tail construct provided by M.J. Tyska (Crawley et al., 2014b). Recombinant proteins were expressed in BL21 (DE3) *Escherichia coli* cells. The N-terminal His_6-tagged proteins were purified using an Ni^{2+}-nitrilotriacetic acid agarose column followed by another step of size-exclusion chromatography (Superdex 200 column from GE Healthcare) in the final buffer of 50 mM Tris-HCl, 1 mM DTT, 1 mM EDTA (pH 7.8), and 100 mM NaCl (low-salt condition) or 500 mM NaCl (high-salt condition). GST-fused proteins were purified by GSH-Sepharose affinity chromatography, followed by a step of size-exclusion chromatography the same as the one described above.

GST Pull-Down Assay

For GST pull-down assays, the GFP-tagged MYO7A CMF and MYO7B CMF were individually expressed in HEK293 cells. GST-tagged NCPDZ3 or GST (2 nmol in 0.9 ml of assay buffer composed of 50 mM Tris-HCl [pH 7.5], 100 mM NaCl, 1 mM EDTA, and 1 mM DTT) was incubated with 0.1 ml of HEK293 cell lysate for 1 hr at 4°C. Next, each mixture was incubated with 30 μl of GSH-Sepharose 4B slurry beads for 30 min, also at 4°C. After washing two times, the captured proteins were eluted by boiling, resolved by 10% SDS-PAGE, and detected by immunoblotting with anti-GFP antibody (Santa Cruz Biotechnology, GFP Antibody [B-2], catalog #sc-9996).

FPLC Coupled with Static Light Scattering

Protein samples (typically 100 μl at a concentration of 20 μM pre-equilibrated with corresponding column buffer) was injected into an AKTA FPLC system with a Superose 12 10/300 Gl column (GE Healthcare) using the column buffer of 50 mM Tris-HCl (pH 7.8), 1 mM DTT, 1 mM EDTA, and 100 mM NaCl (low-salt condition) or 500 mM NaCl (high-salt condition). The chromatography system was coupled to a static light scattering detector (miniDawn, Wyatt) and differential refractive index detector (Optilab, Wyatt). The elution profiles were analyzed using ASTRA 6 software (Wyatt).

Crystallography

Crystals of the ANKS4B SAM-PBM/Harmonin NPDZ1 complex (in 50 mM Tris [pH 7.8], 500 mM NaCl, 1 mM EDTA, and 1 mM DTT buffer) and ANKS4B CEN/MYO7B NMFS complex (in 50 mM Tris [pH 7.8], 100 mM NaCl, 1 mM EDTA, and 1 mM DTT buffer) were obtained by hanging-drop vapor diffusion methods at 16°C. The crystals of the ANKS4B SAM-PBM/Harmonin NPDZ1 complex were grown in buffer containing 3.0 M sodium chloride, 0.1 M bis-Tris (pH 5.5), and soaked in crystallization solution containing 5.0 M sodium chloride for cryoprotection. The crystals of ANKS4B CEN/MYO7B NMFS complex were grown in buffer containing 25% (w/v) pentaerythritol ethoxylate (3/4 EO/OH) and 0.1 M 2-(N-morpholino)ethanesulfonic acid (pH 6.5), and soaked in crystallization solution containing 40% (w/v) pentaerythritol ethoxylate (3/4 EO/OH) for cryoprotection. Diffraction data were collected at the Shanghai Synchrotron Radiation Facility (BL17U or BL19U1) at 100 K. Data were processed and scaled using HKL2000 (Otwinowski and Minor, 1997).

Structure of the Harmonin NPDZ1/ANKS4B SAM-PBM complex was solved by molecular replacement with the model of USH1G/Harmonin complex (PDB: 3K1R) using PHASER (Mccoy et al., 2007). Structure of the ANKS4B CEN/MYO7B NMFS complex was also solved by molecular replacement with models of multiple fragments of the USH1G/MYO7A complex (PDB: 3PVL) as the search model. Further manual model building and refinement were completed iteratively using Coot (Emsley et al., 2010) and PHENIX (Adams et al., 2010). The final model was validated by MolProbity (Chen et al., 2010). The final refinement statistics are summarized in Table S1. All structure figures were prepared by PyMOL (http://www.pymol.org).

Isothermal Titration Calorimetry Assay

ITC measurements were carried out on a VP-ITC Microcal calorimeter (Microcal) at 25°C. Titration buffer contained 50 mM Tris-HCl (pH 7.8), 1 mM DTT, 1 mM EDTA, and 100 mM NaCl (low-salt condition) or 500 mM NaCl (high-salt condition). Each titration point was performed by injecting a 10-μl aliquot of a protein sample from a syringe into a protein sample in the cell at a time interval of 120 s to ensure that the titration peak returned to the baseline. The titration data were analyzed by Origin7.0 (Microcal).

ACCESSION NUMBERS

The atomic coordinates and structure factors of the Harmonin/ANKS4B and ANKS4B/MYO7B complexes have been deposited at the PDB under the accession codes PDB: 5F3X and PDB: 5F3Y, respectively.

SUPPLEMENTAL INFORMATION

Supplemental Information includes six figures and one table and can be found with this article online at http://dx.doi.org/10.1016/j.devcel.2015.12.020.

AUTHOR CONTRIBUTIONS

J.L., Y.H., Q.L., and M.Z. designed experiments and analyzed data. J.L. and Y.H. performed experiments. J.L., Y.H., Q.L., and M.Z. wrote the manuscript. M.Z. coordinated the research.

ACKNOWLEDGMENTS

We thank the Shanghai Synchrotron Radiation Facility (SSRF) BL17U and BL19U1 beamlines for X-ray beam time. We are grateful to Dr. Matthew J. Tyska (Vanderbilt University) for providing the MYO7B CMF construct. This work was supported by grants from RGC of Hong Kong (663811, 663812, 664113, AoE/M09/12, and T13-607/12R) to M.Z. M.Z. is a Kerry Holdings Professor of Science and a Senior Fellow of IAS at HKUST.

Received: October 29, 2015
Revised: December 8, 2015
Accepted: December 21, 2015
Published: January 25, 2016

REFERENCES

Adams, P.D., Afonine, P.V., Bunkoczi, G., Chen, V.B., Davis, I.W., Echols, N., Headd, J.J., Hung, L.W., Kapral, G.J., Grosse-Kunstleve, R.W., et al. (2010). PHENIX: a comprehensive Python-based system for macromolecular structure solution. Acta Crystallogr. D Biol. Crystallogr. *66*, 213–221.

Barr-Gillespie, P.G. (2015). Assembly of hair bundles, an amazing problem for cell biology. Mol. Biol. Cell *26*, 2727–2732.

Bitner-Glindzicz, M., Lindley, K.J., Rutland, P., Blaydon, D., Smith, V.V., Milla, P.J., Hussain, K., Furth-Lavi, J., Cosgrove, K.E., Shepherd, R.M., et al. (2000). A recessive contiguous gene deletion causing infantile hyperinsulinism, enteropathy and deafness identifies the Usher type 1C gene. Nat. Genet. *26*, 56–60.

Boeda, B., El-Amraoui, A., Bahloul, A., Goodyear, R., Daviet, L., Blanchard, S., Perfettini, I., Fath, K.R., Shorte, S., Reiners, J., et al. (2002). Myosin VIIa, harmonin and cadherin 23, three Usher I gene products that cooperate to shape the sensory hair cell bundle. EMBO J. *21*, 6689–6699.

Chen, Z.Y., Hasson, T., Zhang, D.S., Schwender, B.J., Derfler, B.H., Mooseker, M.S., and Corey, D.P. (2001). Myosin-VIIb, a novel unconventional myosin, is a constituent of microvilli in transporting epithelia. Genomics *72*, 285–296.

Chen, V.B., Arendall, W.B., Headd, J.J., Keedy, D.A., Immormino, R.M., Kapral, G.J., Murray, L.W., Richardson, J.S., and Richardson, D.C. (2010).

MolProbity: all-atom structure validation for macromolecular crystallography. Acta Crystallogr. D Biol. Crystallogr. *66*, 12–21.

Crawley, S.W., Mooseker, M.S., and Tyska, M.J. (2014a). Shaping the intestinal brush border. J. Cell Biol. *207*, 441–451.

Crawley, S.W., Shifrin, D.A., Grega-Larson, N.E., McConnell, R.E., Benesh, A.E., Mao, S.L., Zheng, Y.X., Zheng, Q.Y., Nam, K.T., Millis, B.A., et al. (2014b). Intestinal brush border assembly driven by protocadherin-based intermicrovillar adhesion. Cell *157*, 433–446.

El-Amraoui, A., and Petit, C. (2005). Usher I syndrome: unravelling the mechanisms that underlie the cohesion of the growing hair bundle in inner ear sensory cells. J. Cell Sci. *118*, 4593–4603.

Emsley, P., Lohkamp, B., Scott, W.G., and Cowtan, K. (2010). Features and development of Coot. Acta Crystallogr. D Biol. Crystallogr. *66*, 486–501.

Friedman, T.B., Schultz, J.M., Ahmed, Z.M., Tsilou, E.T., and Brewer, C.C. (2011). Usher syndrome: hearing loss with vision loss. Adv. Otorhinolaryngol. *70*, 56–65.

Gillespie, P.G., and Cyr, J.L. (2004). Myosin-1c, the hair cell's adaptation motor. Annu. Rev. Physiol. *66*, 521–545.

Gillespie, P.G., and Muller, U. (2009). Mechanotransduction by hair cells: models, molecules, and mechanisms. Cell *139*, 33–44.

Grati, M., and Kachar, B. (2011). Myosin VIIa and sans localization at stereocilia upper tip-link density implicates these Usher syndrome proteins in mechanotransduction. Proc. Natl. Acad. Sci. USA *108*, 11476–11481.

Hirano, Y., Hatano, T., Takahashi, A., Toriyama, M., Inagaki, N., and Hakoshima, T. (2011). Structural basis of cargo recognition by the myosin-X MyTH4-FERM domain. EMBO J. *30*, 2734–2747.

Johnston, A.M., Naselli, G., Niwa, H., Brodnicki, T., Harrison, L.C., and Gonez, L.J. (2004). Harp (harmonin-interacting, ankyrin repeat-containing protein), a novel protein that interacts with harmonin in epithelial tissues. Genes Cells *9*, 967–982.

Kazmierczak, P., Sakaguchi, H., Tokita, J., Wilson-Kubalek, E.M., Milligan, R.A., Muller, U., and Kachar, B. (2007). Cadherin 23 and protocadherin 15 interact to form tip-link filaments in sensory hair cells. Nature *449*, 87–91.

Kobayashi, I., Imamura, K., Yamada, M., Okano, M., Yara, A., Ikema, S., and Ishikawa, N. (1998). A 75-kD autoantigen recognized by sera from patients with X-linked autoimmune enteropathy associated with nephropathy. Clin. Exp. Immunol. *111*, 527–531.

Kobayashi, I., Imamura, K., Kubota, M., Ishikawa, S., Yamada, M., Tonoki, H., Okano, M., Storch, W.B., Moriuchi, T., Sakiyama, Y., et al. (1999). Identification of an autoimmune enteropathy-related 75-kilodalton antigen. Gastroenterology *117*, 823–830.

Louvard, D., Kedinger, M., and Hauri, H.P. (1992). The differentiating intestinal epithelial-cell—establishment and maintenance of functions through interactions between cellular structures. Annu. Rev. Cell Biol. *8*, 157–195.

Lu, Q., Li, J., and Zhang, M.J. (2014). Cargo recognition and cargo-mediated regulation of unconventional myosins. Acc. Chem. Res. *47*, 3061–3070.

Manor, U., Disanza, A., Grati, M., Andrade, L., Lin, H., Di Fiore, P.P., Scita, G., and Kachar, B. (2011). Regulation of stereocilia length by myosin XVa and whirlin depends on the actin-regulatory protein Eps8. Curr. Biol. *21*, 167–172.

Mathur, P., and Yang, J. (2015). Usher syndrome: hearing loss, retinal degeneration and associated abnormalities. Biochim. Biophys. Acta *1852*, 406–420.

McConnell, R.E., Benesh, A.E., Mao, S., Tabb, D.L., and Tyska, M.J. (2011). Proteomic analysis of the enterocyte brush border. Am. J. Physiol. Gastrointest. Liver Physiol. *300*, G914–G926.

Mccoy, A.J., Grosse-Kunstleve, R.W., Adams, P.D., Winn, M.D., Storoni, L.C., and Read, R.J. (2007). Phaser crystallographic software. J. Appl. Crystallogr. *40*, 658–674.

Mooseker, M.S. (1985). Organization, chemistry, and assembly of the cytoskeletal apparatus of the intestinal brush-border. Annu. Rev. Cell Biol. *1*, 209–241.

Nambiar, R., McConnell, R.E., and Tyska, M.J. (2010). Myosin motor function: the ins and outs of actin-based membrane protrusions. Cell. Mol. Life Sci. *67*, 1239–1254.

Otwinowski, Z., and Minor, W. (1997). Processing of X-ray diffraction data collected in oscillation mode. Methods Enzymol. *276*, 307–326.

Pan, L.F., and Zhang, M.J. (2012). Structures of usher syndrome 1 proteins and their complexes. Physiology (Bethesda) *27*, 25–42.

Pan, L.F., Yan, J., Wu, L., and Zhang, M.J. (2009). Assembling stable hair cell tip link complex via multidentate interactions between harmonin and cadherin 23. Proc. Natl. Acad. Sci. USA *106*, 5575–5580.

Richardson, G.P., de Monvel, J.B., and Petit, C. (2011). How the genetics of deafness illuminates auditory physiology. Annu. Rev. Physiol. *73*, 311–334.

Ridley, A.J. (2011). Life at the leading edge. Cell *145*, 1012–1022.

Schwander, M., Kachar, B., and Muller, U. (2010). The cell biology of hearing. J. Cell Biol. *190*, 9–20.

Sekerkova, G., Zheng, L., Loomis, P.A., Mugnaini, E., and Bartles, J.R. (2006). Espins and the actin cytoskeleton of hair cell stereocilia and sensory cell microvilli. Cell. Mol. Life Sci. *63*, 2329–2341.

Shin, J.B., Krey, J.F., Hassan, A., Metlagel, Z., Tauscher, A.N., Pagana, J.M., Sherman, N.E., Jeffery, E.D., Spinelli, K.J., Zhao, H.Y., et al. (2013). Molecular architecture of the chick vestibular hair bundle. Nat. Neurosci. *16*, 365–374.

Siemens, J., Kazmierczak, P., Reynolds, A., Sticker, M., Littlewood-Evans, A., and Muller, U. (2002). The Usher syndrome proteins cadherin 23 and harmonin form a complex by means of PDZ-domain interactions. Proc. Natl. Acad. Sci. USA *99*, 14946–14951.

Sotomayor, M., Weihofen, W.A., Gaudet, R., and Corey, D.P. (2012). Structure of a force-conveying cadherin bond essential for inner-ear mechanotransduction. Nature *492*, 128–132.

Tilney, L.G., Tilney, M.S., and Derosier, D.J. (1992). Actin-filaments, stereocilia, and hair-cells—how cells count and measure. Annu. Rev. Cell Biol. *8*, 257–274.

Tyska, M.J., Mackey, A.T., Huang, J.D., Copeland, N.G., Jenkins, N.A., and Mooseker, M.S. (2005). Myosin-1a is critical for normal brush border structure and composition. Mol. Biol. Cell *16*, 2443–2457.

Uhlen, M., Fagerberg, L., Hallstrom, B.M., Lindskog, C., Oksvold, P., Mardinoglu, A., Sivertsson, A., Kampf, C., Sjostedt, E., Asplund, A., et al. (2015). Tissue-based map of the human proteome. Science *347*, 1260419.

Verpy, E., Leibovici, M., Zwaenepoel, I., Liu, X.Z., Gal, A., Salem, N., Mansour, A., Blanchard, S., Kobayashi, I., Keats, B.J.B., et al. (2000). A defect in harmonin, a PDZ domain-containing protein expressed in the inner ear sensory hair cells, underlies Usher syndrome type 1C. Nat. Genet. *26*, 51–55.

Wang, C.K., Pan, L.F., Chen, J., and Zhang, M.J. (2010). Extensions of PDZ domains as important structural and functional elements. Protein Cell *1*, 737–751.

Wei, Z., Yan, J., Lu, Q., Pan, L., and Zhang, M.J. (2011). Cargo recognition mechanism of myosin X revealed by the structure of its tail MyTH4-FERM tandem in complex with the DCC P3 domain. Proc. Natl. Acad. Sci. USA *108*, 3572–3577.

Wu, L., Pan, L.F., Wei, Z.Y., and Zhang, M.J. (2011). Structure of MyTH4-FERM domains in myosin VIIa tail bound to cargo. Science *331*, 757–760.

Wu, L., Pan, L.F., Zhang, C.C., and Zhang, M.J. (2012). Large protein assemblies formed by multivalent interactions between Cadherin23 and harmonin suggest a stable anchorage structure at the tip link of stereocilia. J. Biol. Chem. *287*, 33460–33471.

Yan, J., Pan, L.F., Chen, X.Y., Wu, L., and Zhang, M.J. (2010). The structure of the harmonin/sans complex reveals an unexpected interaction mode of the two Usher syndrome proteins. Proc. Natl. Acad. Sci. USA *107*, 4040–4045.

Ye, F., and Zhang, M.J. (2013). Structures and target recognition modes of PDZ domains: recurring themes and emerging pictures. Biochem. J. *455*, 1–14.

Developmental Cell, Volume *36*

Supplemental Information

Mechanistic Basis of Organization of the Harmonin/USH1C-Mediated Brush Border Microvilli Tip-Link Complex

Jianchao Li, Yunyun He, Qing Lu, and Mingjie Zhang

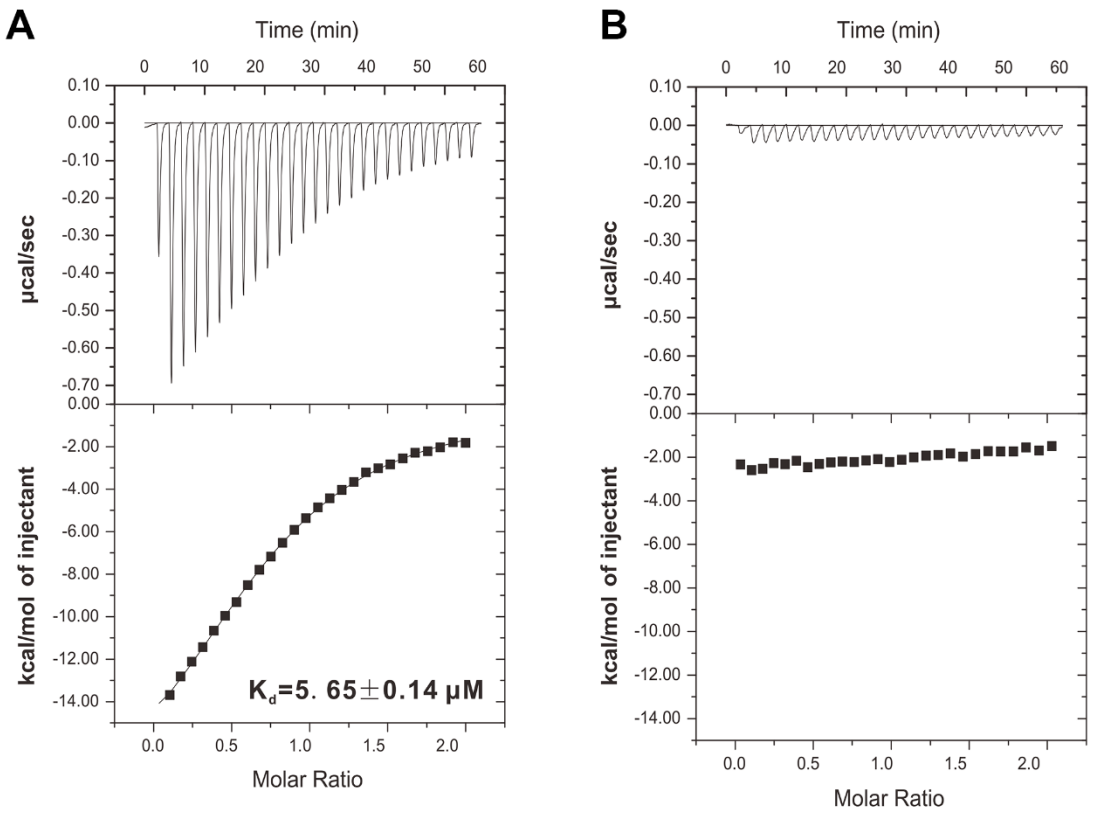

Figure S1. Biochemical characterization of the CDHR2/Harmonin and CDHR5/Harmonin interaction, related to Figure 1.

(A) ITC result showing that CDHR2CD binds to Harmonin with K_d ~5.65 µM. (B) ITC result showing that no interaction can be detected between CDHR5CD and Harmonin.

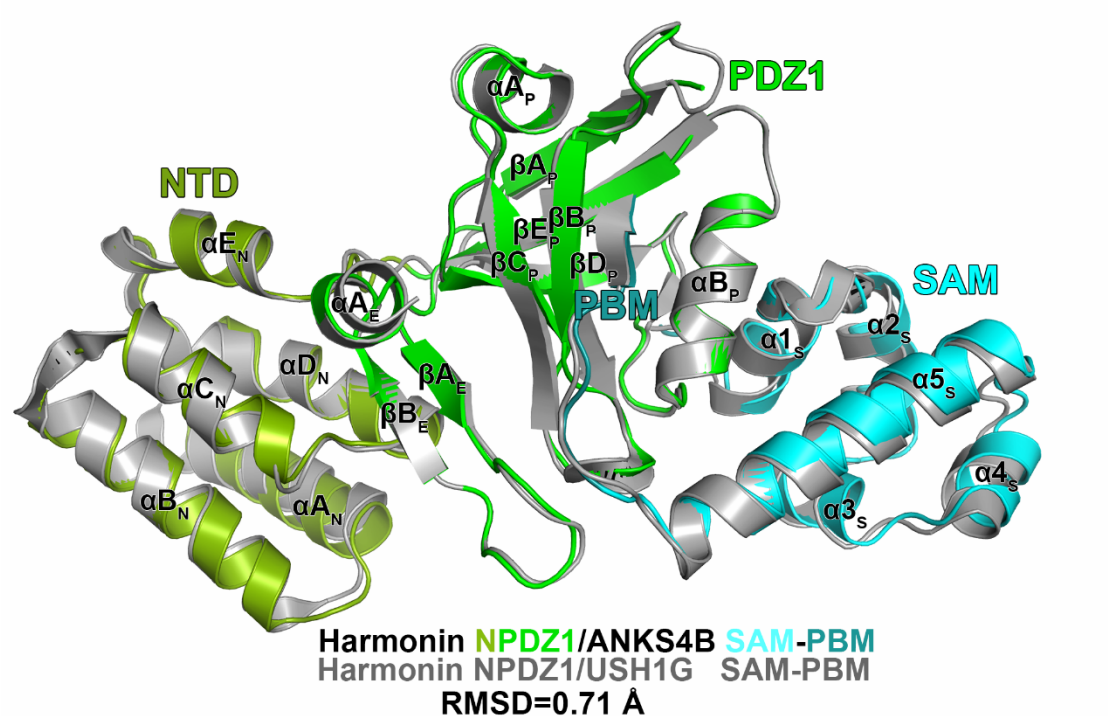

Figure S2. Comparison of the Harmonin NPDZ1/ANKS4B SAM-PBM complex structure and Harmonin NPDZ1/USH1G SAM-PBM, related to Figure 2.
The two structures can be overlapped very well with RMSD of 0.71 Å.

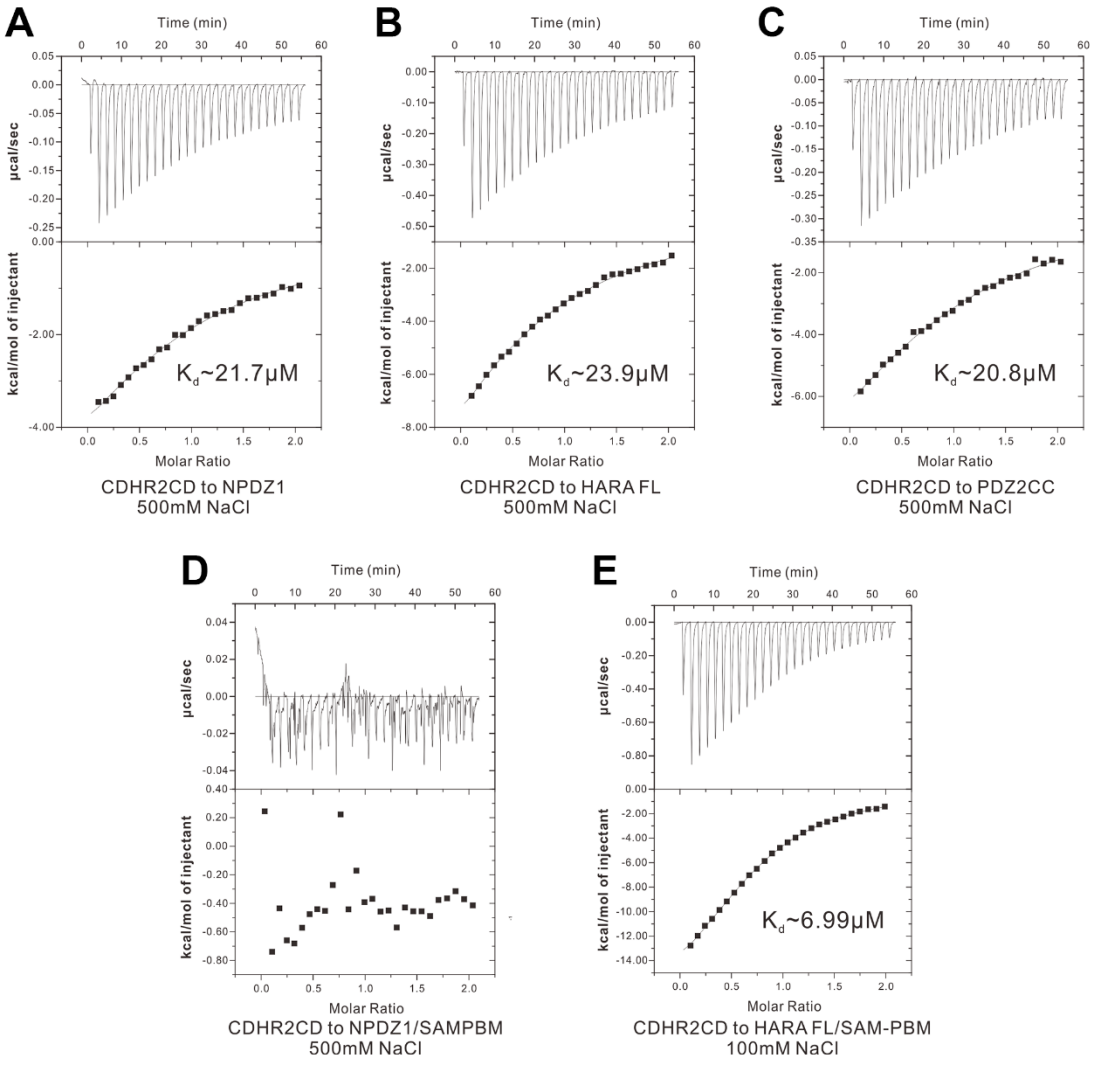

Figure S3. ITC results between CDHR2 and Harmonin under high salt conditions or in the presence of ANKS4B SAM-PBM, related to Figure 2.

(A) CDHR2CD can also bind to NPDZ1 with moderate affinity under high salt conditions. (B) Similar binding affinity can be detected between CDHR2CD and full length Harmonin under high salt condition. (C) The binding affinity decreased about 10 times between CDHR2 and PDZ2CC under high salt condition (1.4 µM *vs* 20.8 µM). (D) ANKS4B SAM-PBM prevent the binding between CDHR2CD and NPDZ1 under high salt condition. (E) ANKS4B SAM-PBM did not affect the binding between CDHR2CD and full length Harmonin.

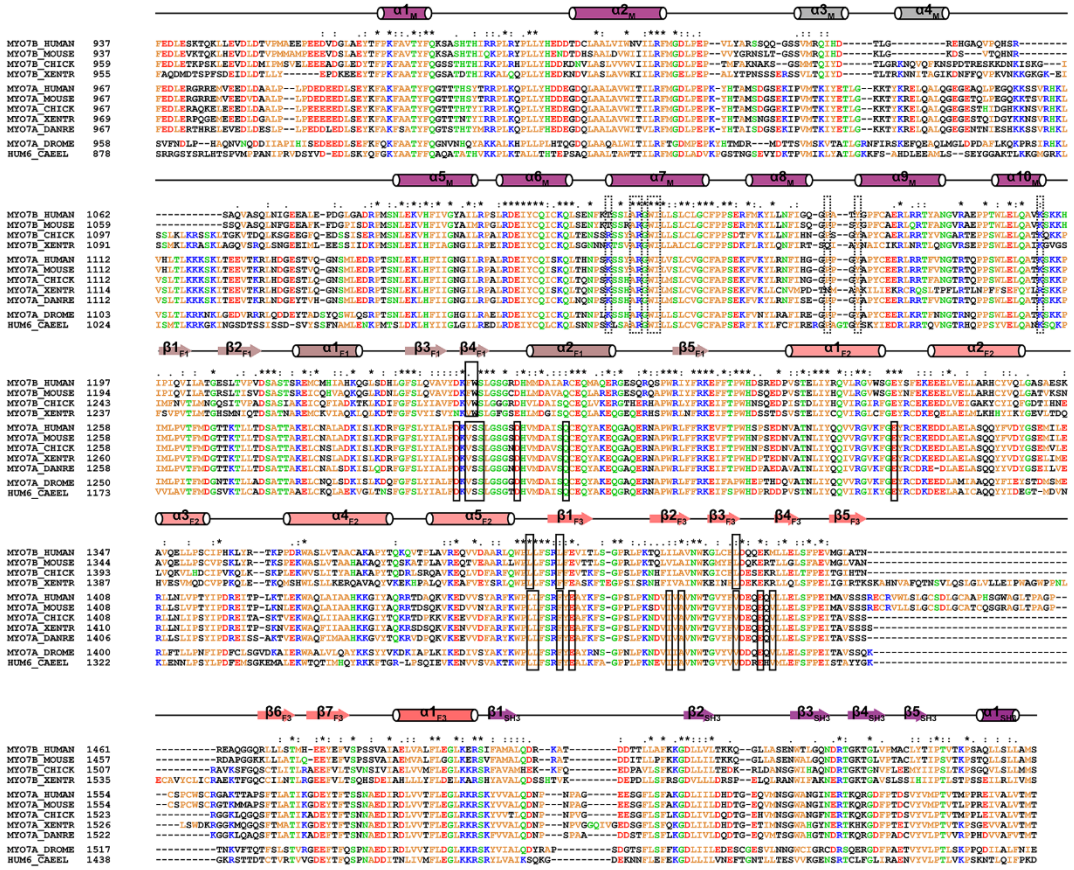

Figure S4. Sequence alignment of NMFS of class VII myosin from different species, related to Figures 3&4.

Identical and highly similar residues are colored (yellow for hydrophobic residues, blue for positively charged residues, red for negatively charged residues and green for other polar residues). Residues involved in CEN2 binding are highlighted with dash box. Residues involved in CEN1 binding are highlighted with black box.

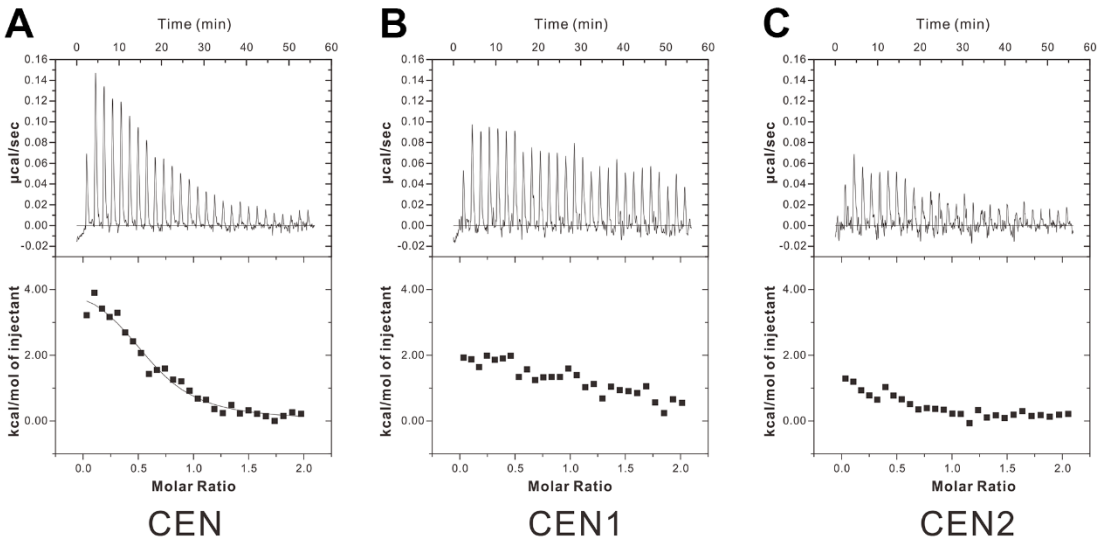

Figure S5. ITC results between different fragments of ANKS4B CEN and MYO7B NMFS, related to Figure 3.

ITC results showing that either CEN1 or CEN2 greatly decreased the binding affinity towards MYO7B NMFS.

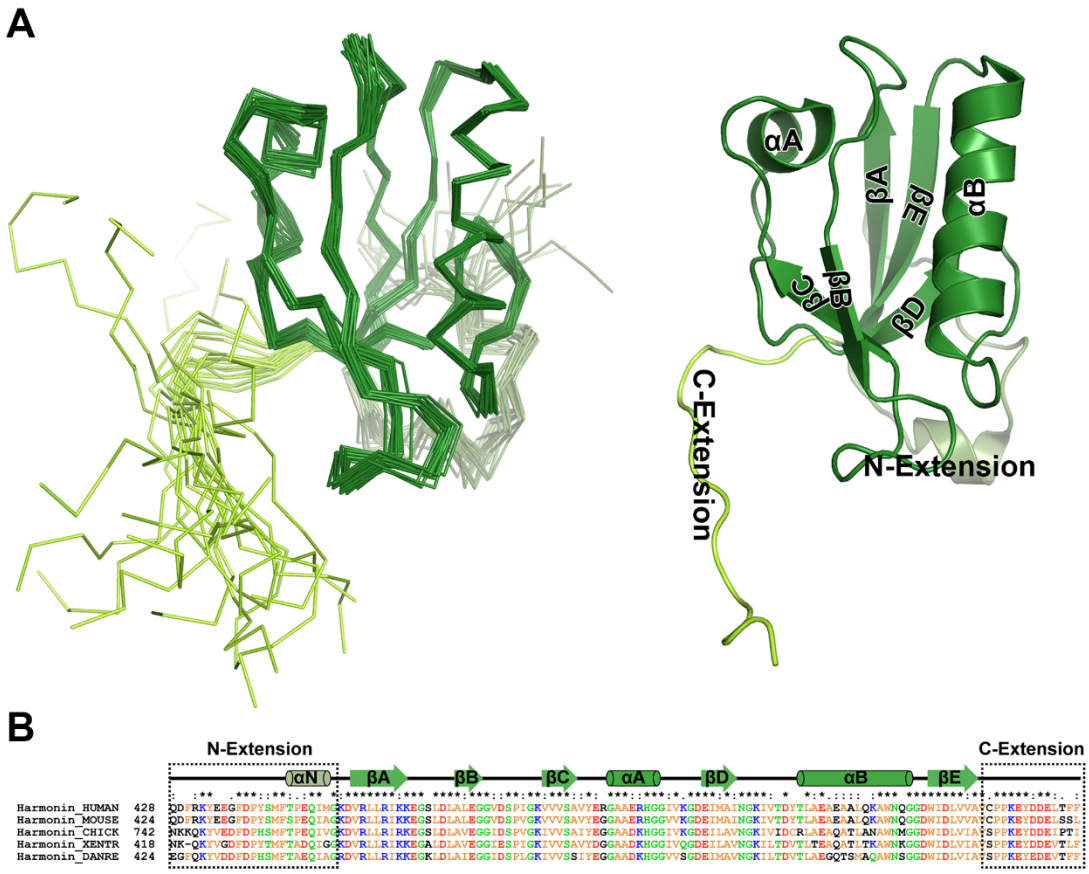

Figure S6. Harmonin PDZ3 contains both N- and C-extension, related to Figure 5.

(A) NMR structure of Harmonin PDZ3 showing that the N-extension forms a short α helix and the C-extension is highly flexible. (B) Sequence alignment showing that the PDZ3 together both the N- and C-extensions are highly conserved across different vertebrate species.

Table S1 Statistics of X-ray Crystallographic Data Collection and Model refinement, related to Figures 2&4.

Data collections

Data sets	Harmonin NPDZ1 + ANKS4B SAM-PBM	MYO7B NMFS + ANKS4B CEN
Space group	$P\ 3_2$	$P\ 4_12_12$
Wavelength (Å)	0.9792	0.9788
Unit Cell Parameters (Å)	a=b=124.57, c=49.65, α=β=90°, γ=120°	a=b=197.52, c=97.71, α=β=γ=90°
Resolution range (Å)	31.5-2.65 (2.70-2.65)	30.72-3.40 (3.46-3.40)
No. of unique reflections	24978 (1264)	24972 (1262)
Redundancy	5.7 (5.5)	6.8 (4.9)
I/σ	38.2 (2.9)	19.6 (2.0)
Completeness (%)	99.5 (100)	92.9 (95.7)
R_{merge} [a] (%)	6.2 (83.6)	10.0 (88.8)
Structure refinement		
Resolution (Å)	31.5-2.65 (2.77-2.65)	30.72-3.40 (3.55-3.40)
R_{cryst} [b]/R_{free} [c] (%)	21.72/26.60 (41.26/50.26)	24.13/28.05 (36.09/38.66)
rmsd bonds (Å) / angles (°)	0.009/1.307	0.008/1.112
Average B factor (Å^2) [d]	80.6	93.2
No. of atoms		
Protein atoms	4055	4041
Other molecules	21	0
No. of reflections		
Working set	23789 (3019)	23493 (2515)
Test set	1133 (154)	1288 (132)
Ramachandran plot regions [d]		
Favored (%)	97.5	96.7
Allowed (%)	2.5	3.1
Outliers (%)	0	0.2

Numbers in parentheses represent the value for the highest resolution shell.

a. $R_{merge} = \Sigma\ |I_i - \langle I \rangle| / \Sigma I_i$, where I_i is the intensity of measured reflection and $\langle I \rangle$ is the mean intensity of all symmetry-related reflections.

b. $R_{cryst}=\Sigma||F_{calc}| - |F_{obs}||/\Sigma F_{obs}$, where F_{obs} and F_{calc} are observed and calculated structure factors.

c. $R_{free}= \Sigma_T||F_{calc}| - |F_{obs}||/\Sigma F_{obs}$, where T is a test data set of about 5% of the total unique reflections randomly chosen and set aside prior to refinement.

d. B factors and Ramachandran plot statistics are calculated using MOLPROBITY (Chen et al., 2010).

References

Chen, V.B., Arendall, W.B., Headd, J.J., Keedy, D.A., Immormino, R.M., Kapral, G.J., Murray, L.W., Richardson, J.S., and Richardson, D.C. (2010). MolProbity: all-atom structure validation for macromolecular crystallography. Acta Crystallogr. D Biol. Crystallogr. *66*, 12-21.